LANGMUIR Article
Cite This: Langmuir 2019, 35, 882–893
pubs.acs.org/Langmuir

Adsorption Behavior of Organic Molecules: A Study of Benzotriazole on Cu(111) with Spectroscopic and Theoretical Methods

Chiara Gattinoni,[†] Panayiotis Tsaousis,[‡] Chanan Euaruksakul,[‡,§] Rachel Price,[‡] David A. Duncan,[§] Tod Pascal,[∥] David Prendergast,[∥] Georg Held,*[,‡,§] and Angelos Michaelides*[,†]

[†]Thomas Young Centre, London Centre for Nanotechnology and Department of Physics and Astronomy, University College London, Gower Street, London WC1E 6BT, U.K.

[‡]Department of Chemistry, University of Reading, Reading RG6 6AD, U.K.

[§]Diamond Light Source, Harwell Science and Innovation Campus, Didcot OX11 0QX, U.K.

[∥]Molecular Foundry, Lawrence Berkeley National Laboratory, Berkeley, California 94720, United States

Supporting Information

ABSTRACT: The adsorption of organic molecules on solid substrates is important to applications in fields such as catalysis, photovoltaics, corrosion inhibition, adhesion, and sensors. The molecular level description of the surface−molecule interaction and of the adsorption structures in these complex systems is crucial to understand their properties and function. Here, we present an investigation of one such system, benzotriazole (BTAH) on single-crystal Cu(111) in vacuum conditions. BTAH is the most widely used corrosion inhibitor for copper and thus a molecule of great industrial relevance. We show that the co-application of a wide range of spectroscopic techniques with theoretical methods provides unique insight in the description of the atomistic details of the adsorbed structures. Specifically, spectroscopic photoemission, absorption, and standing wave experiments combined with ab initio computational modeling allowed us to identify that benzotriazole forms overlayers of intact BTAH when deposited at low temperature, and it dissociates into BTA and H at room temperature and above. The dissociated molecule then forms complex structures of mixed chains and dimers of BTA bound to copper adatoms. Our work also reveals that copper adatoms at low concentrations, such as the theoretically predicted superstructures, cannot be resolved by means of current X-ray photoelectron spectroscopy as the modeled Cu 2p spectra are practically indistinguishable from those for a Cu surface without adatoms. Overall this study significantly deepens understanding of BTAH on Cu, a system studied for more than 50 years, and it highlights the benefits of combining spectroscopic and computational methods to obtain a complete picture of a complex adsorption system.

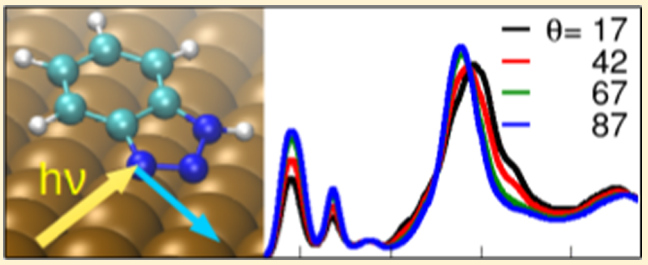

INTRODUCTION

Complex organic molecules have many uses in industry and technology. Their interaction with crystalline surfaces is at the core of a large, and growing, number of applications. A few examples can be found in the fields of engineering, such as in corrosion protection[1] or friction reduction,[2] in energy conversion and storage, where molecule−surface interactions are central to, e.g., dye-sensitized solar cells[3] or in biology, where surface functionalization is needed for many novel biodiagnostics tools.[4] In all cases, an in-depth knowledge of the interface layer between the molecule and the surface is required to understand how the technology itself works. This is however not always achieved, and this lack of understanding is often a barrier to the improvement of these technologies. In the present work, we show how this issue can be addressed via a combination of a variety of spectroscopic techniques and density functional theory (DFT). In particular, we apply these methods to the example of benzotriazole (BTAH) adsorbed on a copper substrate.

Benzotriazole (BTAH, shown in Figure 1) is the most widely used corrosion inhibitor for copper which, like most metals, is subject to tarnishing and corrosion when exposed to a humid atmosphere.[5] It owes its popularity to its efficiency, and it has been consistently used in industrial applications since the 1940s, when it was first synthesized.[6] The reason behind its ability to stop copper from tarnishing and corroding is, however, still elusive despite the large number of research which has been performed over the years to this aim (as reviewed in ref 7). Early experimental studies by means of X-ray diffraction,[8] electrochemical measurements[9] and infrared spectroscopy[10] established that BTAH forms a passivating film by adsorbing on metal or oxidized copper surfaces. The detailed structure of this film and its nanoscale atomistic details have not been unequivocally established, partly because of the

Received: October 24, 2018
Revised: December 18, 2018
Published: January 4, 2019

DOI: 10.1021/acs.langmuir.8b03528
Langmuir 2019, 35, 882−893

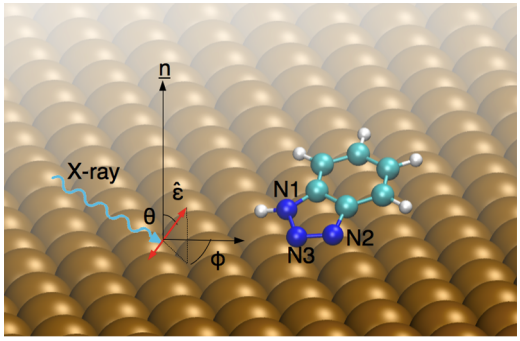

Figure 1. Representation of a BTAH molecule adsorbed on a Cu(111) surface. The BTA molecule differs from the BTAH by the loss of the hydrogen atom in the triazole moiety. On the left-hand side, the quantities used in eq 5 are defined: the polarization of the X-ray ($\hat{\varepsilon}$), the polar angle (θ) and the azimuthal angle (φ).The surface normal $\underline{n}$ is also shown. Cu atoms are copper colored, carbons are cyan, nitrogens blue, and hydrogens white. This color scheme is used throughout.

insolubility of BTAH in aqueous and many organic solutions, which has precluded, until recently, detailed structural and chemical studies.

Recent advances in experimental and computational methods have made it possible to study the adsorption of molecules on surfaces in ultrahigh vacuum (UHV), thus solving the solubility issue and allowing us to focus on the nanoscale details of adsorption. In particular, synchrotron X-ray spectroscopy[11] has revealed the adsorption structure of a wide range of molecules, from simple diatomic to complex ones, on many different substrates. Indeed, single-crystal spectroscopy under ultrahigh vacuum (UHV) conditions can shine a light on the structure of a surface or an adsorbed film without interference from external atmospheric factors. At the same time, on the computational side, density functional theory (DFT) is the go-to tool for the study of adsorbed structures, where the accurate description of intermolecular and molecule−surface bonds is of paramount importance.

Benzotriazole is a complex organic molecule: it can chemisorb to the substrate via the azole moiety, physisorb via the benzene-like ring,[12−15] form complex H-bonded overlayers when intact,[16,17] or instead deprotonate and form structures stabilized by copper adatoms.[16,18−21] The application of some spectroscopic techniques has revealed that under UHV conditions BTAH dissociates into BTA and hydrogen, and that BTA forms ordered structures on the surface.[8,22−27] The experimentally observed variety of structures includes flat-lying chains,[8,22,23] upright chains,[24] upright isolated molecules,[25] and dimers.[26,27] Also on the computational side, chain[16,19−21] or dimer[18] structures consisting of organometallic BTA−Cu complexes have been proposed.

It has been unclear so far whether these discrepancies arise from different experimental conditions, interpretation of the results, or both. In the present work, we show that the adsorption of such a complex organic molecule requires multiple experimental and computational techniques to uniquely identify its adsorbed structure, and the application of one single method will likely lead to an incomplete description of the system. In particular, the interplay between theory and experiment is necessary to identify "hidden" features in the spectra, such as the coexistence of multiple structures or the presence of surface adatoms. Moreover, we highlight that when previous experimental results are reinterpreted in light of our findings, good agreement is generally obtained between the different studies.

In the following, the orientation of the molecules with respect to the surface is investigated using near-edge X-ray absorption fine structure (NEXAFS), chemical bonding using X-ray photoelectron spectroscopy (XPS) and NEXAFS, desorption and dissociation temperatures with temperature-programmed XPS (TP-XPS), and distance of the molecule from the surface with normal incidence X-ray standing wave (NIXSW). DFT is also used to complement and help interpret this suite of experimental techniques. Similar combinations of spectroscopic methods and DFT have been successfully employed to describe the structure of systems of adsorbed molecules on metals such as the interface between liquid water and gold,[28] methyl acetoacetate and nickel,[29,30] ethylene and Si(100),[31] or a dye and ZnO,[32] to name but a few. We restrict our work to Cu(111), as it is the lowest energy surface for copper and thus the dominant face exposed.

The structure of the paper is as follows: the Methodology section introduces the experimental and computational methods; this is followed by the Results, where we show first the temperature-dependent behavior of the adsorbed system, then the structure of the adsorbed layer at 300 K for two BTAH coverages, and finally we investigate the structure of the Cu(111) surface and the presence of Cu adatoms. The Discussion and Conclusions are then presented.

METHODOLOGY

Experimental Section. The experiments were carried out at beamline I09 of the Diamond Light source. The beamline features two canted undulators for soft X-rays (0.1−1.5 keV) and hard X-rays (2.1−15 keV). The endstation has a UHV analysis chamber with a base pressure in the low 10^{-10} mbar range. It is equipped with a Scienta EW4000 HAXPES hemispherical electron energy analyzer with an acceptance angle of ±30°, which was used for X-ray photoelectron spectroscopy, near-edge X-ray absorption fine structure spectroscopy, and normal incidence X-ray standing wave data collection. The analyzer was mounted at an angle of 90° (83°) with respect to the hard (soft) X-ray beam in the plane of the photon polarization.

The Cu single crystal was clamped onto a heater plate, which was mounted on a liquid nitrogen-cooled cold finger, thus allowing heating and cooling between 120 and 900 K. The Cu(111) surface was cleaned by repeated cycles of Ar sputtering at room temperature and annealing to 900 K until all contaminants' XPS signals were below the detection limit (<0.01 multilayer (ML)). The benzotriazole layers were deposited prior to the spectroscopy experiments in a preparation chamber which can be separated from the analysis chamber and allows transfer in vacuum. Prior to dosing, benzotriazole (Sigma-Aldrich, purity 99%) was heated to 55 °C in a pumped test tube and thoroughly degassed. At this temperature, the vapor pressure is high enough to dose 100% saturation quantities directly onto the surface through a needle valve connected to the UHV chamber. Benzotriazole was dosed at pressures in the 10^{-8} mbar range.

XPS spectra in the C 1s, N 1s, and Cu 2p regions were recorded at 10° off-normal emission using photon energies of 420, 515, and 1080 eV, respectively. The binding energies (BEs) were calibrated with respect to the Fermi energy which was determined by measuring spectra of the Fermi edge using

DOI: 10.1021/acs.langmuir.8b03528
Langmuir 2019, 35, 882−893

the same parameters (monochromator settings, pass energy, etc.). In addition, the spectra were normalized with respect to the low BE background. The overall energy resolution for the XPS data shown here is around 0.2 eV. Fast temperature-programmed (TP-)XPS spectra were recorded, while the sample was annealed at a rate of 0.1 K s^{-1} (6.1 K per spectrum). C and N K edge NEXAFS spectra were recorded using the KLL Auger electron yields integrated over the kinetic energy ranges 252.5−267.5 and 372.5−383.5 eV, respectively. Spectra of the clean surface were subtracted from those of the adsorbate-covered surfaces. The N K edge spectra were then divided by the beamline flux (I_0) measured with a gold mesh inserted in the beamline. The C K edge spectra were divided by the integrated signal of the Cu 3p XPS peak, measured with the same photon energy, as the I_0 signal showed features of carbon contamination. Even with this procedure, however, features due to contamination of the beamline optics could not be removed completely and/or discriminated from genuine adsorbate-induced features, especially in the pre-edge region. All spectra shown here were normalized at 320 and 425 eV, respectively.

The normal incidence X-ray standing wave (NIXSW[33]) measurements were performed in the same endstation. The integrated intensity of the N 1s photoemission peaks was used to monitor the relative X-ray absorption of the N atoms. The photoemission spectra were acquired in a fixed energy mode with a pass energy of 500 eV. A calibration curve was generated by dividing a fixed energy mode scan by a swept energy mode scan with the same step size, and comparable acquisition time acquired over an area of the XP spectrum that was comparably flat. This calibration curve was used to normalize the N 1s photoemission spectra, which were then fitted with a linear background and four Gaussian line shapes corresponding to the two chemically unique N species in the adsorbed molecule (see below) and two shake-up energy loss features. Nondipolar effects, due to the angular dependence of the photoemission, were modeled using theoretically calculated values, as described in ref 34 and in the Supporting Information. The NIXSW measurements were repeated five times on different spots of the sample, and the absorption profiles were fitted separately to produce an average value for the coherent fraction, f_{coh}, and coherent position, p_{coh}, and the associated random uncertainty. f_{coh} and p_{coh} are defined through the following equation

$$f_{coh}\ \exp(2\pi i p_{coh}) = \sum_n f_n\ \exp(2\pi i p_n) \qquad (1)$$

The sum runs over all absorber atoms contributing to the respective N 1s peak. p_n are the positions of N atoms above the (111) scattering planes in modulo units of the separation between the (111) planes of Cu atoms (d_{111} = 2.08 Å); f_n are relative coverages (corrected by the Debye−Waller factor to account for thermal deviations from the ideal positions) of these atoms.[33]

Simulation. Simulated NEXAFS spectra and XPS core level shifts were calculated using DFT-based methods for the most stable BTA(H)/Cu(111) structures identified in previous publications.[16,18,19] In addition, a new upright monomer configuration has also been considered (see Figure 2a). A variety of four-layer-thick (unless otherwise stated) cell sizes were used. Most low-coverage structures were modeled using a 4 × 4 Cu(111) slab, except for the dimers (chains) where a 2 × 7 (5 × 4) system was used. For the high-coverage case, a 2 × 4 slab was employed for all structures except the chains, where a 2 × 5 one was used. All of the structures have been optimized using Vienna Ab initio Simulation Package (VASP),[35−38] with the optB86b-vdW functional[39] and the projector-augmented wave (PAW) method.[40] The kinetic energy cutoff on the basis set was 400 eV, and the Monkhorst−Pack grids of 3 × 3 × 1 (2 × 6 × 1/ 6 × 3 × 1) k-points were used for the 4 × 4 and 5 × 4 (2 × 7/ 2 × 4 and 2 × 5) cells. Periodic images were separated by ∼20 Å vacuum, and the bottom Cu layer coordinates were kept fixed at bulk values. Convergence of all the settings has been thoroughly checked.[16] Adsorption at low coverage was modeled between 1/16 and 1/7 ML, at high coverage between 1/5 and 1/4 ML, where 1 ML refers to one molecule per surface Cu atom. Adsorption energies, E_{ads}, in Figure 2 are calculated as

$$E^{\alpha}_{ads} = E_{system} - N_{BTAH}E_{BTAH} - E_{slab} - \alpha\Delta N_{Cu}g_{Cu} \qquad (2)$$

where E_{BTAH} and E_{slab} are, respectively, the total energies of the BTAH molecule in the gas phase and of the substrate (with Cu

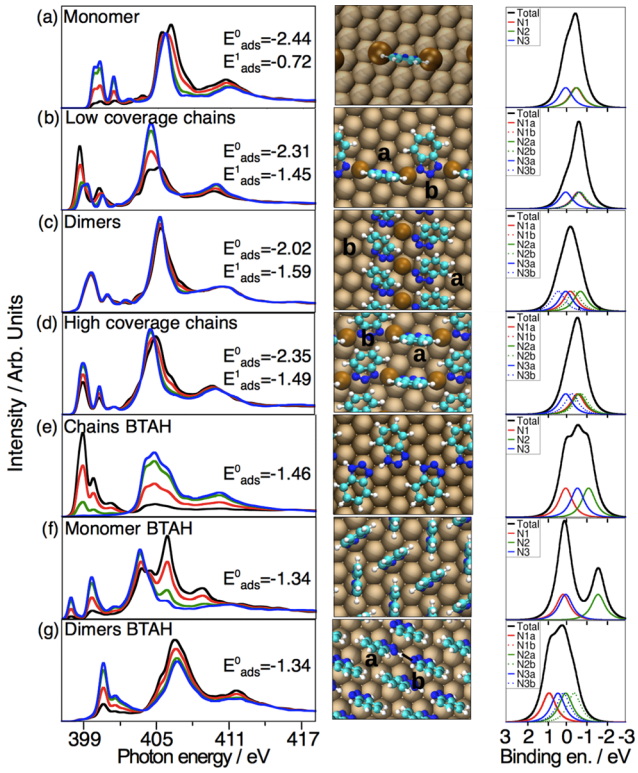

Figure 2. Simulated N K edge NEXAFS (left) and simulated N 1s XPS (right) spectra for the BTA structures considered in this work, shown in the middle column. (a) Low coverage BTA monomer stabilized by two Cu_{ad}; (b) low-coverage BTA chains (1/10 ML); (c) high-coverage BTA chains (1/5 ML); (d) BTA dimers (1/7 ML for low coverage, 1/4 ML for high coverage); (e) low-coverage BTAH (1/16 ML); (f) high-coverage BTAH dimers (1/4 ML); (g) high-coverage BTAH monomers (1/4 ML). The dark brown atoms on top of the Cu(111) surface (depicted in light brown) are copper adatoms. The NEXAFS spectra have been calculated for θ = 17 (black), 42 (red), 67 (blue), 87° (green), where θ is the angle between the polarization and the normal to the surface. In the structural figures (middle panels), the *a* and *b* labels indicate molecules *a* and *b* in the corresponding XPS spectra. N1, N2, and N3 are defined in Figure 1. In the XPS spectra, the N atom closer to the surface has its calculated spectrum centered at 0. Adsorption energies are calculated according to eq 2.

DOI: 10.1021/acs.langmuir.8b03528
Langmuir 2019, 35, 882−893

adatoms). E_{system} is the total energy of the whole system, consisting of BTAH adsorbed on the Cu slab, for an intact structure, and of BTA and H co-adsorbed on the substrate, for the deprotonated case. N_{Cu} is the number of adatoms, and g_{Cu} the calculated formation energy. The parameter α can take the value 0 (the adatoms are present on the surface prior to adsorption) or 1 (all adatoms have to be formed from the copper bulk). A thorough examination of the cost of adatom formation and how that affects the stability of the systems is presented in the Supporting Information (SI).

XPS core level shifts for N 1s and Cu 2p were calculated with VASP in the final state approximation (screening by the valence electrons is included only) using the modified PAW method.[41] The core electron binding energy is calculated as the difference between the total energies of the final (excited) state and the initial (ground) state

$$E_B = E_f - E_i \tag{3}$$

The specific quantity reported herein is the binding energy shift, ΔE_B, relative to a reference system

$$\Delta E_B = E_B^{sys} - E_B^{ref} \tag{4}$$

where E_B^{ref} is the binding energy for an excited atom chosen as reference and E_B^{sys} for the excited atom of interest. The model XPS spectra were generated from the shifts by the superposition of the Gaussian−Lorentzian (G/L) peaks (Gaussian−Lorentzian products) with 50% mixing and full width at half-maximum (FWHM) 0.95 eV (N 1s) and 0.80 eV (Cu $2p_{3/2}$), as determined from fits to the experimental data. These were weighed with the number of atoms for each species.

The NEXAFS spectra for the nitrogen and carbon K edges were simulated using the excited-electron core−hole (XCH) method,[42] which has been custom-built into the Quantum-ESPRESSO package.[43] The core−hole excitation is imposed by replacing the ground state pseudopotential with a core-excited one derived from a constrained electronic structure configuration (e.g., $1s^1 2s^2 2p^4$ for nitrogen). The X-ray adsorption cross-section is calculated using Fermi's golden rule, whose transition matrix ($\underline{\boldsymbol{A}}$) elements are calculated within the projector-augmented wave approximation.[44] The θ-dependent spectra (where θ is the angle between the polarization direction and the surface normal, see Figure 1) are finally obtained via a two-dimensional (2D) isotropic average of the cross-section

$$\begin{aligned} I(\theta) &= \frac{1}{2\pi}\int_0^{2\pi} \hat{\epsilon}\cdot\underline{\boldsymbol{A}}\cdot\hat{\epsilon}\, d\phi \\ &= \frac{1}{2}(xx + yy)\sin^2(\theta) + zz\cos^2(\theta) \end{aligned} \tag{5}$$

In the above, $\hat{\epsilon}$ is the polarization vector, ϕ the polar angle, θ the azimuthal angle, and xx, yy, zz the diagonal elements of the transition matrix $\underline{\boldsymbol{A}}$. The directions are defined as the xy plane being parallel to the surface and the z axis perpendicular and corresponding to $\theta = 0$. Similar to the XPS calculations, the excitation energies obtained from this DFT-based method deviate significantly from the experimental values. To match the simulated spectra with the experimental ones, a shift is applied such that the first peak of the π^*-resonance corresponds to the first peak in the experimental data. Calculations were performed on the preoptimized structures (with VASP, as described above) at the Γ point, and a generalized implementation[45] of the Shirley k-space interpolation scheme[46] is used for Brillouin zone sampling. The Perdew−Burke−Ernzerhof exchange−correlation functional,[47] Vanderbilt ultrasoft pseudopotentials,[48] and a plane-wave basis set with a kinetic energy cutoff of 25 Ry (340 eV) were used. For comparison and validation, XPS core shifts were calculated also with the XCH method. The shifts obtained with VASP and XCH presented the same trends, and the maximum differences observed in ΔE_B were of the order of 50 meV. This highlights that the two methods used for the calculations in this study are compatible.

RESULTS

Adsorption Models for Benzotriazole on Cu(111). In this section, we use DFT to examine the adsorption energies and spectroscopic features for possible adsorption geometries of benzotriazole on Cu(111). All of the computed spectra reported herein are new. The structures shown in Figure 2 (and, with more details, in Figure S1) are taken from a large pool of previously published candidate structures.[16,18,19] Only the most stable structures were considered for this work, as explained in detail in the SI. Although it is expected that the molecule is deprotonated (i.e., BTA) at room temperature, we also consider BTAH structures. The most stable BTAH configurations are shown in Figure 2e for low coverage and Figure 2f,g for high coverage. For BTA, we only consider the monomer (Figure 2a), chains (Figure 2b), and dimers (Figure 2c) for low coverage and stacked chains (Figure 2d) and dimers (Figure 2c) at high coverage. Figure 2 also lists the respective adsorption energies as well as calculated N K edge NEXAFS and N 1s XPS spectra. C 1s XPS spectra were not calculated, as the chemical environment of the carbon atoms is largely the same in all model structures, namely, an aromatic ring not directly interacting with the surface. Therefore, no significant differences are expected.

The most stable adsorption structures are those of BTA in the presence of surface copper adatoms (Cu_{ad}) acting as a link between neighboring BTAs (Figure 2b−d) or stabilizing the BTA on the surface (Figure 2a). In general, the presence of copper adatoms allows a larger number of strong Cu−N bonds to be formed by the N atoms in the triazole moiety, whereby one nitrogen binds to a Cu atom within the surface layer and one (BTA dimer) or both (BTA monomer, chains) other nitrogens form bonds with the Cu adatoms. Structures of BTAs adsorbed on Cu(111) without Cu adatoms had been investigated in refs 16, 21 where they were found to be unfavorable with respect to the intact structures presented in Figure 2. They are therefore not considered in this study. The structures of the low- (Figure 2b) and high-coverage (Figure 2d) BTA chains both consist of alternating upright and tilted molecules forming three N−Cu bonds each. The tilting of every second BTA in the chain structure is coverage-dependent, being almost flat at low coverage and ∼60° with respect to the surface plane at high coverage. The BTA−Cu_{ad}−BTA dimers (Figure 2c) consist of nearly upright molecules tilted (∼60° with respect to the surface) each forming two N−Cu bonds, one with a Cu atom within the surface plane and one with an adatom. The dimers have the same structure at low and high coverages, the only difference being the lateral spacing between neighboring chains (therefore only one structure is shown in Figure 2c). Because of the similar chemical environment of all three nitrogen atoms, DFT predicts only small chemical shifts of less than 1 eV in the N 1s XP-spectra for all of the BTA structures. In the chains, at both

DOI: 10.1021/acs.langmuir.8b03528
Langmuir 2019, 35, 882−893

coverages, only the central N3 atoms (the definitions of N1, N2, and N3 are shown in Figure 1) of both triazoles show a significant shift as they are the only N not binding strongly to a Cu adatom (Figure 2b,d). The computed shifts in binding energy for these N3 atoms are however only 0.64 eV (at low coverage) and 0.58 eV (at high coverage) higher with respect to the other nitrogens. For the dimers, the binding energies are equally spaced out for the six nitrogens examined, the range of binding energies being 0.8 eV.

The simulated N K edge NEXAFS spectra for the BTA structures show two absorption peaks about 1.5 eV apart, which are both associated with the π^* system. The more intense peak at low photon energy is narrow for the chain structures (Figure 2b,d), broader for the dimer (Figure 2c), and split for the monomer structures (Figure 2a). This reflects the different levels of N−Cu bonding in these structures. The σ^* system shows two distinct peaks at about 6 and 12 eV above the first π^*-resonance. The angular dependence of both π^*- and σ^*-resonances is as expected for a system dominated by resonant N═N and N═C double bonds with the respective orientations.[49] The upright monomer structure (Figure 2a) is characterized by a strong angular dependence in the π^*-resonance with the highest cross-section close to normal incidence (θ = 90°). One component of the first σ^*-resonance peak shows the opposite behavior, whereas the other features are largely unaffected by the changes in the polarization vector. The angular dependence expected for the low-coverage chain structure (Figure 2b) is almost opposite to that of the monomer with the highest absorption cross-section for the main π^*-resonance peak at grazing incidence (θ = 17°). The cross-section does not go to zero for normal incidence and instead a shoulder grows, which is due to the fact that the structure consists of two molecules with different orientations. Both σ^*-resonance peaks show the opposite angular behavior. The high-coverage chain structure (Figure 2d) leads to a more moderate angular dependence as the tilt of one of the two molecules in the structure is close to the "magic angle" of 54.7°, for which no angular dependence is expected. For the same reason, the dimer structure (Figure 2c) shows almost no angular dependence in the modeled NEXAFS spectra.

The Boltzmann probability distribution for these structures (shown in Figure S2 of the Supporting Information) shows that every one of them is favorable for different conditions of the surface (i.e., whether the surface is more or less disordered with many or few adatoms), and therefore they all have to be carefully considered.

The character of the adsorption structures for non-deprotonated BTAH (Figure 2e−g) changes according to the coverage. At low-coverage (1/16 ML), the most stable structures consist of H-bonded chains with the BTAHs lying almost parallel to the surface (Figure 2e). At high coverage (1/4 ML), all of the BTAHs are upright, and their adsorption is stabilized by the formation of N−Cu bonds. Two isoenergetic structures are observed: a monomer structure with no hydrogen bonds (Figure 2f) and a H-bonded dimer configuration (Figure 2g). Structures with higher coverages are unstable. Therefore, 1/4 ML can be considered as the saturation coverage for BTAH. As the protonated nitrogen atom has a different chemical environment from the other N atoms, larger chemical shifts are predicted for the BTAH structures, compared to BTA, and this is shown in the broader XPS spectra in Figure 2e−g. In the low-coverage chains, the N1 atoms (which are part of the N−H in the triazole, see Figure 1) have the highest binding energy and the N2 ones (which form a H-bond with the neighboring BTAH) the lowest. Their calculated binding energies are ∼0.6 eV either side of the central N3 atom and 1.15 eV apart. The monomer (Figure 2f) shows two distinct peaks almost 2 eV apart: one for N1 and N3 and a second for N2 which is neither bonded to the triazole H (N1) nor to the surface (N3). Finally, in the dimers (Figure 2g), the peaks corresponding to the six N atoms of the structure are fairly spread apart over 1.5 eV, with the N1 atoms having the highest binding energies.

The simulated N K edge NEXAFS spectra for BTAH at low coverage (Figure 2e) show a π^* system composed of three distinct peaks ∼1.5 eV apart, which reflect the three chemical environments of the triazole nitrogen atoms: one involved in a H-bond, the central one in a N−Cu bond, and one bonded to a H-atom. The σ^* system shows two distinct peaks with opposite angular dependence with respect to the π^*-resonance, i.e., the highest intensities are for grazing incidence in the π^*-resonance and normal for the σ^*. At high coverage, the spectra for the monomer (Figure 2f) show two π^* peaks of similar intensity spaced ∼1 eV apart and a σ^* system with two peaks and a node. In the case of the dimer (Figure 2g), there is instead a single peak with a shoulder for π^* and two distinct peaks for σ^*. In both spectra, the highest intensity for the π^*-resonance is at normal incidence and for the σ^* at grazing angles.

Temperature-Dependent Behavior of the Adsorbed System. The temperature dependence of the benzotriazole layer on Cu(111) was studied by means of XPS and TP-XPS. In particular, the onset of deprotonation into BTA and H, desorption, and decomposition were investigated. When dosing benzotriazole at 320 K, the intensities of the C 1s and N 1s XPS spectra saturate after 5 min (Figure 3). Indeed, the 8 min spectrum (dashed red line) and the 5 min one (solid red line) are identical. We define this layer as the saturated

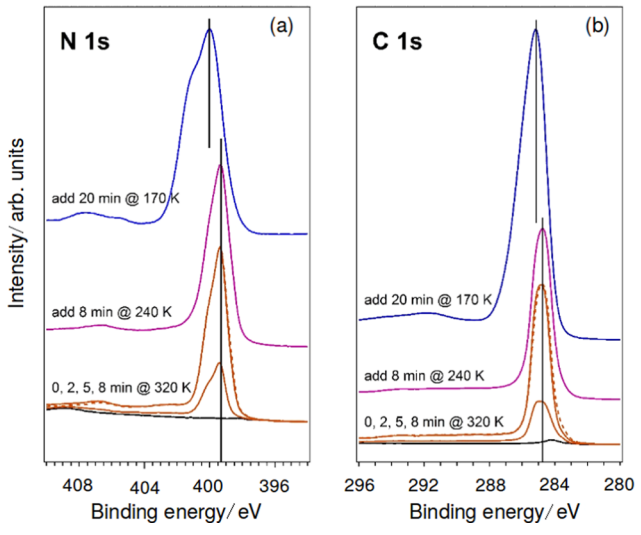

Figure 3. Measured XPS spectra for different levels of benzotriazole uptake and temperatures. (a) N 1s (photon energy 515 eV), (b) C 1s (photon energy 420 eV). The spectra at the bottom of the figure (black line) are for a nominally clean surface. The red lines correspond to dosing times of 2 min, 5 min (solid), and 8 min (dashed) at 320 K; the purple spectrum in the middle corresponds to an additional 8 min dosing at 240 K; the blue spectrum at the top corresponds to an additional 20 min dosing at 170 K.

DOI: 10.1021/acs.langmuir.8b03528
Langmuir 2019, 35, 882−893

chemisorbed layer and use the relative intensities of the respective N 1s signals for coverage calibration of all other BTA layers studied in this work. Comparison of both the C 1s and N 1s peak intensities consistently leads to a coverage of 30% saturation for the 2 min spectrum. The C 1s spectra at 320 K show a single peak at BE 284.8 eV, which is consistent with carbon atoms in an organic system. The N 1s signal has a main peak at 399.4 eV, a shoulder at 400.3 eV, which is more pronounced for the low-coverage spectrum (2 min) than for saturation coverage, and a satellite feature around 407 eV. Additional dosing at 240 K does not increase the coverage significantly except for a small additional asymmetry at the high binding energy side of the main signal. Dosing at 170 K, however, leads to multilayer growth, and the main peaks of the spectra shift by about 0.5 eV with respect to the chemisorbed species. After dosing for 20 min at 170 K, the Cu 2p signal is completely attenuated (<1% of clean surface signal, not shown). Using the inelastic mean free path for 150 eV electrons through glassy C (7.5 Å),[50] we estimate that the layer is at least 35 Å thick.

Figure 4 shows N 1s spectra recorded for 36 and 100% saturated layers at 300 K. We find good qualitative agreement between the experimental XPS spectra and the model spectra for low- and high-coverage BTA chains or dimers, which are also shown in Figure 4. The experimental spectra are broader, however they contain the same features as the calculated ones, i.e., a main peak with a shoulder at high BE, which is more pronounced for the low coverage than for 100% saturation coverage. The narrow distribution of N 1s binding energies of less than 1 eV in the experimental spectra clearly rules out the presence of BTAH on the surface, which would lead to broad or multiple features spread over 2−3 eV (see Figures 2 and 4).

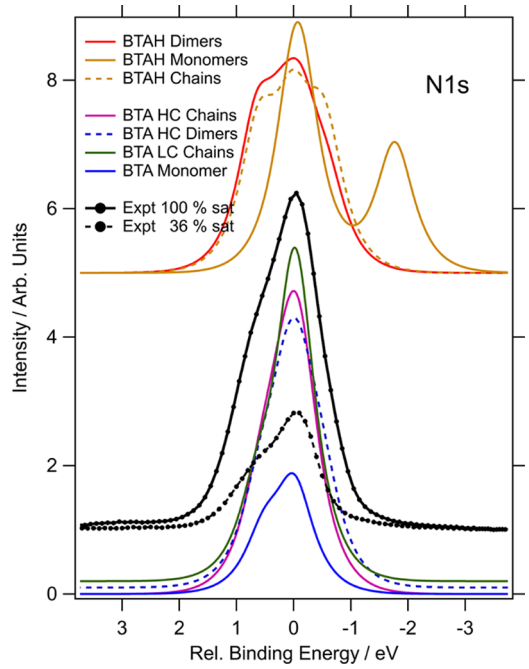

Figure 4. Comparison of experimental (100 and 36% saturation) and computational N 1s XPS spectra. Experimental data are shown as dots with lines. Calculated spectra are shown as solid and dashed lines. In all of the spectra, the 0 of the relative binding energy corresponds to the position of the peak with the highest intensity.

TP-XPS reveals further insights into the thermal evolution of the benzotriazole layer. After dosing the equivalent of 114% of the saturated chemisorbed layer onto the clean surface at 280 K (Figure 5b), very significant differences are observed in the N 1s signal compared to the layer dosed at 320 K (Figure 3a) which are lifted once the sample is annealed to 320 K (Figure 5a,b). These observations are explained by intact adsorption of benzotriazole (BTAH) at 280 K and reordering of the layer and dissociation into BTA and H upon annealing. Three distinct peaks at 399.2, 400.2, and 401.3 eV are visible in the 281 K spectrum of Figure 5b. Our model calculations show that this is a signature of high-coverage BTAH (see Figure 4). At 320 K, the spectrum shows a single peak with a shoulder, as described above, which is in good agreement with theoretical predictions for deprotonated BTA (see Figure 4). The specific BTA structure formed at room temperature at high coverage will be discussed in the following section. Between 320 and 430 K, the signal changes very little reflecting the stability of the surface layer, before desorption and decomposition of the molecules starts above 430 K (as previously observed[51]). Between 430 and 670 K, the signals of intact BTA at BE 399.3 eV and a decomposition feature with a N 1s peak at 398.0 eV co-exist. The temperature dependence of the total N 1s signal (see Figure 5c) shows that the signal of the intact BTA molecule is decreasing by 87% over this temperature range, whereby 24% of the signal is lost in the final desorption step between 640 and 670 K. After annealing to 670 K, the intensity of the decomposition peak at 398.0 eV is only about 30% of the N 1s signal of BTA at 320 K (BE 399.3 eV). At the same time, the total N 1s signal decreases by 60%, i.e., about 60% of the molecules desorb, whereas 40% decompose, and their N atoms remain on the surface.

It has been previously reported[52] that benzotriazole can reduce the rate of oxidation of copper in air up to a temperature of ∼620 K. This is consistent with these results showing that benzotriazole or its dissociation products cover the surface up to this temperature.

Adsorption at 300 K. *Deprotonation.* The XPS spectra discussed in the previous section show that benzotriazole is deprotonated at room temperature. To add support to this conclusion, the structure of benzotriazole deposited at 50 and 100% saturation on Cu(111) was studied with NEXAFS, both for the N and the C K edge. The combination of the experimental measurements and their comparison to DFT-optimized structures and calculated spectra allows us to conclude that the adsorbed overlayer consists of deprotonated BTA for both coverages. Indeed, the experimental N K edge spectra show π^*-resonances at excitation energies between 398 and 401 eV and σ^*-resonances at energies above 402 eV (Figures 6a and 8a). For both coverages, for the π^*-resonance, two clearly resolved peaks are observed, and the σ^* system has two features about 5 eV apart. As the calculated spectra for BTAH predict a third peak in the π^* system (chains, Figure 2e) or a very different character in the σ^* system (monomer and dimers, Figure 2f,g), this indicates that at 300 K benzotriazole is deprotonated into BTA and H.

Model C K edge spectra for all candidate structures are shown in Figure S2 of the Supporting Information. They all show two equally intense π^*-resonance peaks (except for the BTAH monomer, where one main peak is observed instead), 1.2−1.7 eV apart. The lower excitation energy is associated with π states within the C_6-ring; the higher energy peak is an excitation in π-states near the C═N bonds. The experimental

DOI: 10.1021/acs.langmuir.8b03528
Langmuir 2019, 35, 882−893

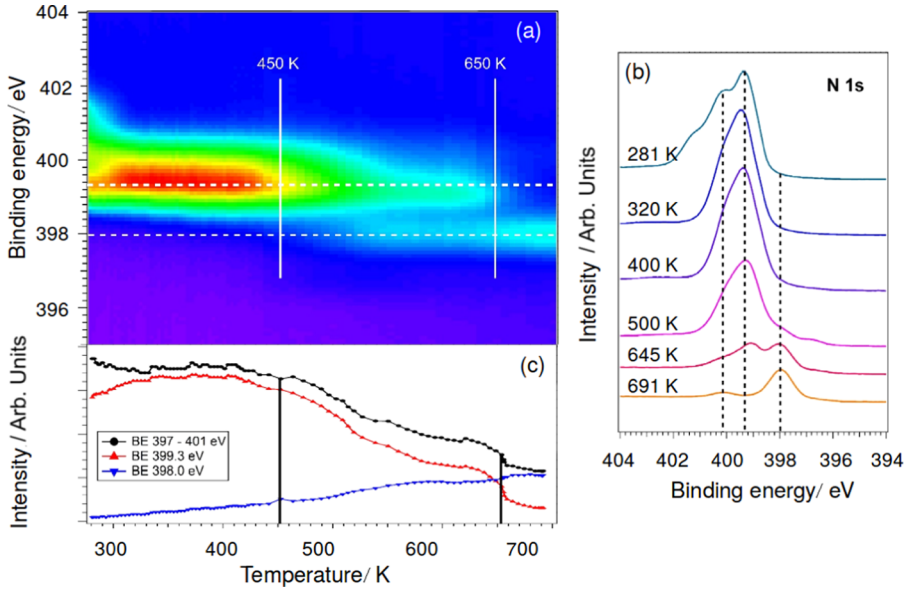

Figure 5. (a) Two-dimensional (2D) plot showing the temperature dependence of the experimentally measured XPS signal. (b) Single measured XPS spectra for a range of temperatures between 281 and 691 K. (c) Temperature dependence of the total N 1s signal between 397 and 401 eV (black line), the signal at 399.3 ± 0.4 eV (intact molecule, red line) and 398.0 ± 0.4 eV (decomposition product, blue line).

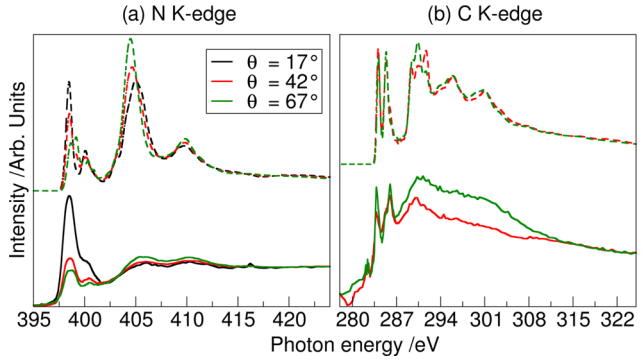

Figure 6. Comparison of experimental and computational spectra for the (a) N K edge and (b) C K edge for low-coverage BTA adsorption at 300 K. Experimental data are shown as solid lines. The computational spectra (dashed lines) are those for a mixture of 25% upright monomers (Figure 2a) and 75% low-coverage chains (Figure 2b). The angle θ refers to the angle between the X-ray polarization vector and the surface normal (see Figure 1).

C K edge spectra recorded at 300 K for both 50 and 100% saturation coverage show two π^*-resonance peaks (Figures 6b and 8b, solid lines), which is in good agreement with most of the model spectra, dissociated and intact. Therefore, the C K edge does not provide information regarding dissociation, which is expected as the loss of the H-atom does not significantly affect the chemical environment of the benzene-like ring.

Structure at Low Coverage. NEXAFS spectra for the N and C K edge (θ = 17, 42, 67°) were collected for benzotriazole deposited at 50% saturation, and they are shown as solid lines in Figure 6. These were compared to theoretical spectra for all structures described in the previous section and shown in Figure 2, and the best fit is shown as dashed lines in Figure 6.

The highest intensity for the N K edge (Figure 6a) is observed for θ = 17°, indicating that there is a significant number of flat-lying molecules present at the surface. The low-coverage chain structure in Figure 2b is the only deprotonated case where the calculated NEXAFS spectra show the highest π^* cross-section for low values of θ. The low-coverage chains alone provide good agreement with the experimental data.

However, the C K edge spectra suggest that a mixed adsorption structure of chains and upright monomers (up to 30%) might be a better fit. Indeed, the angular dependence of the π^* region in the experimental C spectra (Figure 6b, solid lines) is more in line with an upright orientation of the C_6-ring, contrary to the results obtained from the N K edge. None of the theoretical spectra showed opposite angular dependence between N and C K edge, as expected, since the π^* orbitals are perpendicular to the plane of the molecule in both cases. In addition, one would expect that at least some of the σ^*-resonances show an opposite behavior to the π^*-resonance, which is not observed in these experimental spectra. Compared to the N K edge, the data collection of C K edge NEXAFS spectra is more challenging because carbon contamination of the beamline optical elements results in very significant drops in the beamline transmission in this spectral region. Despite best efforts with normalization, this can cause artificial features and large errors in relative intensities. It can therefore not be excluded that the relative intensities and, thus, the angular dependence is affected by artifacts in the normalization procedure.

Alternatively, this result could suggest that the structure is a mixture of flat and upright geometries contributing differently to the spectra of the two different edges. Indeed, adding between 25 and 35% of upright monomers to the system does not alter the character of the N K edge, however it reverses the angular dependence of the π^*-resonances in the C K edge, as shown in Figure 6b. We can therefore conclude that low-coverage BTA chains are dominant in the low-coverage adsorption of benzotriazole on Cu(111), however 25−35% of upright monomers might also be present.

Structure at High Coverage. The structure of benzotriazole deposited at 100% saturation on Cu(111) was studied with NEXAFS, both for the N and the C K edge, and NIXSW. Although NEXAFS is capable of determining bond angles,

DOI: 10.1021/acs.langmuir.8b03528
Langmuir 2019, 35, 882−893

NIXSW allows the determination of the height of atoms above a single-crystal surface. Therefore, the combination of the two techniques provides a more complete picture of the system.

NIXSW data were acquired for the saturated chemisorbed BTA layer dosed at 320 K (for 9 min). A detailed description of the data analysis and representative experimental data are included in the Supporting Information. All DFT models predict a wide distribution of heights of carbon atoms within the aromatic rings, which are all contributing to the single C 1s peak at 284.8 eV. Therefore, these positions cannot be determined by NIXSW. The number of nitrogen atoms is smaller, their height distribution narrower, and there is a clear shift in binding energy between different species, which makes the determination of their positions far more viable. Figure 7

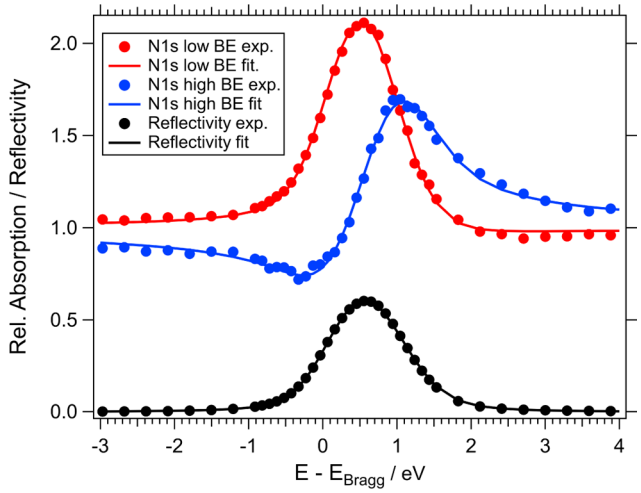

Figure 7. Experimental data and fits to the NIXSW Bragg reflection (black curve) and peak intensity curves of the two resolved N 1s peaks (red: low BE signal; blue high BE signal).

shows the energy dependence of the low and high BE N 1s peaks (399.4 and 400.3 eV) and the reflectivity curve together with fits. The coherent fractions, f_{coh}, and positions, p_{coh}, resulting from the fits (and calculated using eq 1) are listed in Table 1 together with values expected for different BTA model geometries using the coordinates from the DFT-optimized structures in Figure 2. The fit to the absorption curve of the low BE peak yields a very low coherent fraction of 0.28, which is indicative of either disorder or atoms in different positions contributing to this peak. Typical values for atoms at a single position are around 0.9. A comparison with the values expected for the DFT model geometries shows that only the BTA dimers model leads to a similar coherent fraction for this peak, however the coherent positions and f_{coh} for the high BE peaks do not match as well. Better agreement can be achieved by mixing dimer and chain structures, and the results for mixed BTA low-coverage chains and BTA dimers geometries are listed in the lower part of Table 1. Satisfying agreement with the experimental data is achieved for mixtures between 30:70% and 35:65%. It should be noted that the coherent fraction can be significantly affected by small levels of contamination and beam damage, which cannot be completely ruled out in these experiments. Therefore, one expects a larger discrepancy between experiment and model in these values. The experimental error bars stated in Table 1 are based to the variance of the fits to different data sets and do not include such systematic errors.

Experimental NEXAFS spectra for the N and C K edge were obtained for θ = 17, 42, 67, 87°, and they are shown in Figure 8 as solid lines. The dashed lines are the best theoretical fit

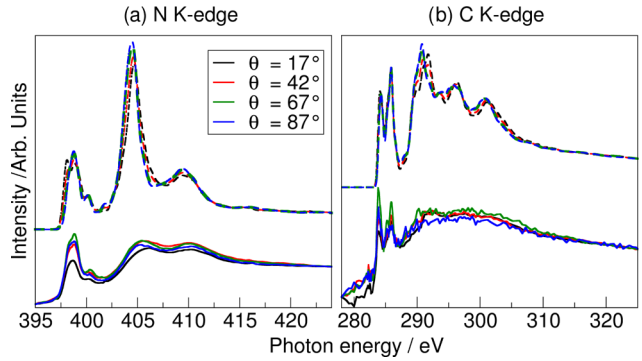

Figure 8. Comparison of experimental and computational spectra for the (a) N K edge and (b) C K edge for high-coverage BTA adsorption at 300 K. Experimental data are shown as solid lines. The computational spectra (dashed lines) are those for a mixture of 30% low-coverage chains (Figure 2b) and 70% dimers (Figure 2c). The angle θ refers to the angle between the X-ray polarization vector and the surface normal (see Figure 1).

Table 1. Coherent Fractions, f_{coh}, and Positions, p_{coh} (in Units of d_{111}), Determined from the Fits to the NIXSW Absorption Curves for the Low and High BE N 1s Peaks and Values Expected for Different Models, As Described in the Text[a]

	low BE peak (399.4 eV)		high BE peak (400.3 eV)	
	f_{coh}	p_{coh}	f_{coh}	p_{coh}
experiment	0.28 ± 0.03	0.36 ± 0.01	0.68 ± 0.02	0.95 ± 0.01
single geometry models				
BTA monomer	0.99	0.37	1.00	0.01
BTA dimers	0.29	0.16	0.99	0.89
BTA LC chains (LCC)	0.99	0.37	0.41	0.17
BTA HC chains (HCC)	0.94	0.39	0.98	0.07
mixed geometry models				
20% LCC + 80% dimers	0.34	0.26	0.78	0.91
30% LCC + 70% dimers	0.39	0.28	0.69	0.92
35% LCC + 65% dimers	0.43	0.30	0.63	0.93
40% LCC + 60% dimers	0.47	0.31	0.59	0.93
50% LCC + 50% dimers	0.55	0.33	0.50	0.96

[a]The error bars of the experimental data are determined from the variance between different experiments.

DOI: 10.1021/acs.langmuir.8b03528
Langmuir 2019, 35, 882−893

after comparison with the structures in Figure 2 and the NIXSW findings. The theoretical spectra, which are shown, correspond to the 30% low-coverage chains and 70% dimers mixture, which is the best fit with the NIXSW data. Good agreement between this structure and the experimental data is obtained. For the N K edge (Figure 8a), the experimental data shows two distinct π^*-resonance peaks and broad σ^* features ~5 eV apart. Although the position of the π^* peaks is the same for all angles, 398.8 and 400.3 eV, a small shift is observed in the positions of the σ^* peaks, from 406.1 eV for small incidence angles ($\theta = 17°$) to 405.3 eV at high incidence angles ($\theta = 87°$). It is worth noting that the angle dependence of the π^*- and σ^*-resonance peaks is also in good agreement with the computed spectra of the high-coverage chains (see Figures 2d and S2d). Therefore, without the extra information provided by NIXSW, the spectra could instead be assigned to this very different structure. We can thus conclude that the high-coverage structure of benzotriazole on Cu(111) consists of dissociated BTA mostly arranged in dimers and partially as chains of alternating upright and flat molecules.

Adatoms on the Cu(111) Surface. As the chemical shifts in XPS strongly depend on the coordination of the emitter atoms, one would expect a significant shift in the binding energy of the Cu 2p photoelectrons emitted from the Cu adatoms with respect to the bulk signal. To our knowledge, the only experimental value available for a Cu $2p_{3/2}$ surface core level shift is that of Cu layers of variable thickness on a Ni(111) surface, $\Delta E_B^{exp} = -0.31$ eV.[53]

Our calculations for the surface layer of a seven-layer thick Cu(111) slab yield a surface core level shift of $\Delta E_B = -0.28$ eV with respect to the bulk atoms, which is in very good agreement with the experimental value.[53] Copper adatoms on the same slab (with no other adsorbates) lead to $\Delta E_B \sim -0.71$ eV (see Table 2, bottom). When BTA molecules are present on the surface, the binding energy shifts for the adatoms are reduced, or can even change sign, depending on the structure (see Table 2, top), leading to values between $\Delta E_B = -0.53$ eV and 0.60 eV. This indicates different levels of charge transfer through the N−Cu_{ad} bonds, which appears strongest for the dimers ($\Delta E_B = 0.60$ eV). The calculated core level shifts of the Cu atoms within the surface layer deviate very little from that of the flat clean Cu(111) surface, with values between −0.25 and −0.17 eV.

Table 2. Calculated Chemical Shifts, ΔE_B, of the Cu $2p_{3/2}$ Levels for Surface Atoms and Copper Adatoms (Cu_{ad}) with respect to the Bulk ($\Delta E_B = 0$ eV)[a]

structure	Cu_{ad}		surface
BTA LC chains	−0.50	−0.43	−0.21
BTA dimers	+0.60		−0.17
BTA HC chains	−0.34	−0.53	−0.25
Cu slab flat			−0.28
Cu slab w. adatoms	−0.71	−0.70	−0.28

[a]All values are in electronvolt. Two copper adatoms are present in the unit cell of the chains and only one Cu_{ad} for the dimers.

Model spectra were calculated by a weighed superposition of the Gaussian−Lorentzian peaks (G/L mixing 90%; FWHM 0.8 eV, as determined from the experimental data), shifted by the respective values for the adatoms, surface layer, and first bulk layers (assuming an inelastic mean free path of 5.6 Å[50]). The comparison of model spectra for different models shows that the signal from the adatoms becomes virtually indiscernible from the spectrum expected for the clean surface (see Figure 9) due to the low concentration of copper adatoms (the Cu_{ad}/Cu_{slab} ratio is 1/6 at its most dense). Within the experimental error and, more importantly, due to the uncertainties imposed by intensity variations caused by photoelectron diffraction, it is, therefore, not possible to confirm the presence of Cu adatoms, nor their absence, in this adsorption structure by comparing experimental and model spectra.

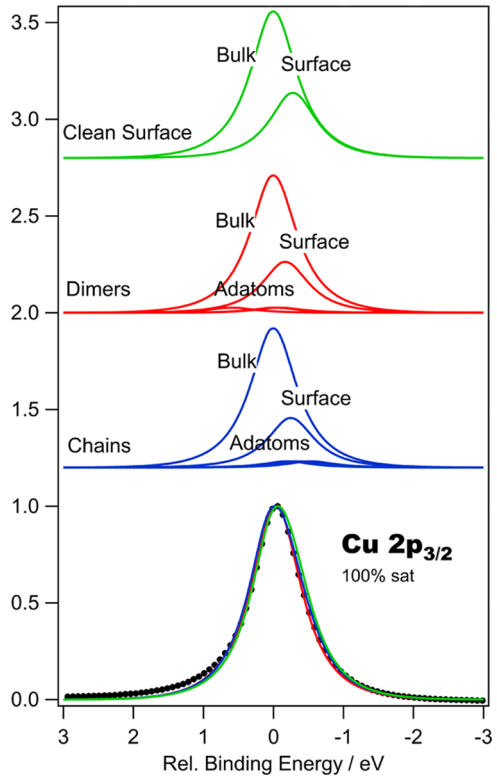

Figure 9. Comparison of experimental (black dots) and model Cu $2p_{3/2}$ spectra for the two high-coverage systems of deprotonated BTA with high density of Cu_{ad}, high-coverage chains (blue lines), high-coverage domains (red lines), and the clean Cu(111) surface without adatoms (green lines). The peaks representing the individual contributions to the spectra are plotted in the upper part of the Figure, the combined model spectra (superposition of all individual peaks) are plotted together with the experimental data.

DISCUSSION

In the present work, we have shown that a combination of spectroscopic techniques and DFT calculations provides a detailed description of the adsorption of a complex organic molecule on a substrate. In particular, we have studied benzotriazole on Cu(111) for a wide range of temperatures and at two coverages, providing new insight into its adsorption behavior. The benzotriazole/Cu system has long been studied; a variety of structures have been reported in the literature, at seemingly similar conditions, thus prompting the need for further work to improve our understanding of this system and to bring clarity to previous results. In the present work, we used a combination of synchrotron-based spectroscopic experimental techniques (NEXAFS, XPS, TP-XPS, NIXSW) and DFT.

DOI: 10.1021/acs.langmuir.8b03528
Langmuir 2019, 35, 882−893

We shed a light on the structure of the adsorbed film of the substrate and on the temperature evolution of the system. We have identified that up to 280 K, benzotriazole forms adsorbed layers of intact BTAH on Cu(111). At room temperature, the molecule is dissociated into BTA and H, confirming the results of previous studies at room temperature in UHV.[25−27,54] Previous computational work has also shown that deprotonated adsorbed systems of benzotriazole are more stable,[16,19] and that the energy barrier for deprotonation is relatively low at below 1 eV.[55]

Both at low and high coverages, complex structures with coexisting different molecular arrangements are observed. At low coverage, the predominant structure is chains of alternating upright and flat BTAs (Figure 2b). An excess of ∼30% of upright molecules with respect to flat-lying ones might also be present, and they might appear either at the end of the low-coverage chains or interspersed between the chains. At high coverage, a structure composed primarily of highly packed dimers is observed, and around 30% of low-coverage chains coexist. A combination of techniques was found necessary to identify these structures unambiguously. XPS, which was used to probe the local chemical environment of the N atoms, gave theoretical spectra with relatively small differences between the different structures considered. It was thus sufficient to determine the protonation state of the molecule but not the exact overlayer structure. The latter was obtained through NEXAFS, probing the orientation of molecular orbitals, and NIXSW, providing information on the molecule−surface bond lengths. Both were needed to correctly identify the high-coverage structures as predominantly dimers rather than high-coverage chains.

The copper adatoms, which are vital to stabilize these chain and dimer structures, are not detected via XPS. We have shown that despite significant chemical shifts of around 0.5 eV, the low Cu_{ad} concentration renders their contribution to the overall Cu 2p XPS signal insignificant. However, having established that benzotriazole is dissociated (through the comparison of experimental and theoretical XPS and NEXAFS spectra), its presence can be inferred by previous DFT work, which has shown[16] (see also Figure S6) that the adsorption of BTA on Cu(111) is only favorable when it is aided by Cu adatoms.

Previous experimental studies of high-coverage benzotriazole in UHV on Cu(111) have also shown a mostly upright adsorption of the molecules through the azole moiety, however they differ from each other and the present study in the predicted overlayer structure. Fang et al.[24] predicted a structure of upright chains connected by H-bonds between neighboring benzene and azole rings. The H-bond is, however, supposed to be very weak in this configuration,[56] and the structure itself has subsequently been contested.[54] The newly proposed structure in ref 54 is instead of almost upright BTAs connected by copper adatoms, possibly forming chains. NEXAFS results by Walsh et al.[25] also suggested an almost upright adsorption of (deprotonated) single upright BTAs on the Cu(100) surface. The data from these studies and from the present work do agree with the orientation of high-coverage BTA, i.e., almost upright. These previous results can be re-read in light of the present findings, and a good agreement across the board is obtained. In fact, the NEXAFS spectra of ref 25 are very close to those obtained in the present study, and thus could be reinterpreted in the same way. In ref 54, XPS and UV photoelectron spectroscopy show that deprotonated BTA adsorbs via the triazole moiety, and that the orientation of the molecule is slightly tilted with respect to the surface normal. Similarly, ref 24 reports deprotonation, the plane of the molecule tilted from the surface, and possible BTA−Cu polymerization. Again, these results are consistent with the present findings.

Finally, the dimer structures found to be prevalent in our study have also been observed by Grillo et al.,[26,27] by means of scanning tunneling microscopy. A significant difference, however, between the present work and ref 26 is the prevalence of the dimers also at low coverage, rather than chains. This could be due to differences in the surface condition. Figure S1 shows that the conditions of the surface can affect which Cu_{ad}-aided structures are favorable, dimers being expected when the energy cost of forming the adatoms is very high. It could thus be possible that this set of experiments fall into this range especially since the surface in ref 26 is reconstructed. Despite it being quite unusual, adsorbate-induced reconstructions have been observed for Cu(111).[57−60] Although the cause for the reconstruction is unknown in this case, its presence could have two important consequences: it could make the surface atoms less mobile, thus disfavoring the presence of adatoms at the sites needed to form chains and it could provide templating effects which again could favor dimers over chains.

The present work also showed that the compact, high-coverage layer of dissociated BTA is stable up to at least 450 K. Since dissociated BTA is strongly adsorbed to the surface,[16,18−21] this molecular "barrier" can perform a protective action toward Cu(111) via a competitive adsorption mechanism.[7] The protective action of the BTA overlayer against corrosion can be expected up to 670 K when complete desorption or decomposition is observed. The layer, however, becomes steadily less stable from 430 K, when desorption and decomposition start being appreciable, and thus corrosion inhibition is expected to decrease in this temperature range. This is in good agreement with previous findings of benzotriazole reducing oxidation of copper up to ∼620 K.[10,52]

■ CONCLUSIONS

The present work demonstrates that the synergy between several spectroscopic techniques and DFT calculations is necessary to reveal complex details of this system of organic molecules on a substrate. Indeed, DFT has helped clarify seemingly contradictory N and C NEXAFS spectra for low-coverage adsorption, showing them to be compatible with an excess of upright molecules in the system, which is however dominated by chains. Similarly, the combinations of NEXAFS, NIXSW, and DFT leads to the identification of a dimer/chain mixture as the high-coverage structure, rather than the theoretically more energetically stable chains. This combination of techniques has also been pivotal in clarifying the experimental finding of a seemingly "clean" surface, i.e., without copper adatoms, observed with XPS. Indeed, DFT has shown that a distinct surface feature such as copper adatoms, resulting in theoretical XPS shifts on the order of ∼0.5 eV, does not affect the overall XPS spectra at the concentration needed in the adsorbed systems.

DOI: 10.1021/acs.langmuir.8b03528
Langmuir 2019, 35, 882−893

■ ASSOCIATED CONTENT

Supporting Information

The Supporting Information is available free of charge on the ACS Publications website at DOI: 10.1021/acs.langmuir.8b03528.

Theoretical NEXAFS and XPS spectra and formation energies for all of the BTAH and BTA adsorption models; description of the NIXSW data analysis procedure and sample data (PDF)

■ AUTHOR INFORMATION

Corresponding Authors

*E-mail: g.held@reading.ac.uk (G.H.).
*E-mail: angelos.michaelides@ucl.ac.uk (A.M.).

ORCID

Chiara Gattinoni: 0000-0002-3376-6374
David A. Duncan: 0000-0002-0827-2022
Georg Held: 0000-0003-0726-4183
Angelos Michaelides: 0000-0002-9169-169X

Notes

The authors declare no competing financial interest.

■ ACKNOWLEDGMENTS

A.M.'s work is partly supported by the European Research Council under the European Unions Seventh Framework Programme (FP/2007-2013)/ERC Grant Agreement no. 616121 (HeteroIce project). The authors are grateful for computational resources to UCL research computing, the U.K. Car-Parrinello Consortium UKCP (EP/F036884/1), for access to Archer, and the Materials and Molecular Modelling Hub, which is partly funded by EPSRC (EP/P020194/1). The calculation of the theoretical NEXAFS spectra used resources of the National Energy Research Scientific Computing Center (NERSC), a U.S. Department of Energy Office of Science User Facility operated under Contract No. DE-AC02-05CH11231. C.G. performed part of this work as a user project at the Molecular Foundry which is supported by the Office of Science, Office of Basic Energy Sciences, of the U.S. Department of Energy under Contract No. DE-AC02-05CH11231. Diamond Light Source is acknowledged for access to beamline I09, technical and travel support under beamtime award SI12800. The authors particularly acknowledge the help of Tien-Lin Lee, Pardeep Kumar Thakur, and David McCue during the experiments. P.T. acknowledges part-funding for a Ph.D. studentship from Diamond Light Source.

■ REFERENCES

(1) Kuznetsov, Y. I.; Mercer, A. D.; Thomas, J. G. N. *Organic Inhibitors of Corrosion of Metals*; Springer: New York, 1996.
(2) Spikes, H. Friction Modifier Additives. *Tribol. Lett.* **2015**, *60*, 5.
(3) Nazeeruddin, M. K.; Baranoff, E.; Grätzel, M. Dye-sensitized solar cells: A brief overview. *Sol. Energy* **2011**, *85*, 1172−1178.
(4) Howes, P. D.; Rana, S.; Stevens, M. M. Plasmonic nanomaterials for biodiagnostics. *Chem. Soc. Rev.* **2014**, *43*, 3835−3853.
(5) Gattinoni, C.; Michaelides, A. Atomistic details of oxide surfaces and surface oxidation: the example of copper and its oxides. *Surf. Sci. Rep.* **2015**, *70*, 424−447.
(6) Procter & Gamble, Ltd. Compositions for Inhibiting Metal Tarnish. British Patent 652339, 09 Dec, 1947.
(7) Finšgar, M.; Milošev, I. Inhibition of copper corrosion by 1,2,3-benzotriazole: A review. *Corros. Sci.* **2010**, *52*, 2737−2749.
(8) Dugdale, I.; Cotton, J. B. An electrochemical investigation on the prevention of staining of copper by benzotriazole. *Corros. Sci.* **1963**, *3*, 69−74.
(9) Cotton, J. B.; Scholes, I. R. Benzotriazole and Related Compounds as Corrosion Inhibitors For Copper. *Br. Corros. J.* **1967**, *2*, 1−5.
(10) Poling, G. Reflection infra-red studies of films formed by benzotriazole on Cu. *Corros. Sci.* **1970**, *10*, 359−370.
(11) Nefedov, A.; Wöll, C. In *Surface Science Techniques*; Bracco, G., Holst, B., Eds.; Springer: Berlin, Heidelberg, 2013; p 277.
(12) Kokalj, A.; Peljhan, S. Density Functional Theory Study of ATA, BTAH, and BTAOH as Copper Corrosion Inhibitors: Adsorption onto Cu(111) from Gas Phase. *Langmuir* **2010**, *26*, 14582−14593.
(13) Kokalj, A.; Kovačević, N.; Peljhan, S.; Finšgar, M.; Lesar, A.; Milošev, I. Triazole, Benzotriazole, and Naphthotriazole as Copper Corrosion Inhibitors: I. Molecular Electronic and Adsorption Properties. *ChemPhysChem* **2011**, *12*, 3547−3555.
(14) Peljhan, S.; Kokalj, A. DFT study of gas-phase adsorption of benzotriazole on Cu(111), Cu(100), Cu(110), and low coordinated defects thereon. *Phys. Chem. Chem. Phys.* **2011**, *13*, 20408−20417.
(15) Jiang, Y.; Adams, J. B. First principle calculations of benzotriazole adsorption onto clean Cu(111). *Surf. Sci.* **2003**, *529*, 428−442.
(16) Gattinoni, C.; Michaelides, A. Understanding corrosion inhibition with van der Waals DFT methods: the case of benzotriazole. *Faraday Discuss.* **2015**, *180*, 439−458.
(17) Finšgar, M.; Lesar, A.; Kokalj, A.; Milošev, I. A comparative electrochemical and quantum chemical calculation study of BTAH and BTAOH as copper corrosion inhibitors in near neutral chloride solution. *Electrochim. Acta* **2008**, *53*, 8287−8297.
(18) Chen, X.; Hakkinen, H. Divide and Protect: Passivating Cu(111) by Cu-(benzotriazole)$_2$. *J. Phys. Chem. C* **2012**, *116*, 22346−22349.
(19) Kokalj, A.; Peljhan, S.; Finsgar, M.; Milosev, I. What Determines the Inhibition Effectiveness of ATA, BTAH, and BTAOH Corrosion Inhibitors on Copper? *J. Am. Chem. Soc.* **2010**, *132*, 16657−16668.
(20) Kokalj, A. Ab initio modeling of the bonding of benzotriazole corrosion inhibitor to reduced and oxidized copper surfaces. *Faraday Discuss.* **2015**, *180*, 415−438.
(21) Peljhan, S.; Koller, J.; Kokalj, A. The Effect of Surface Geometry of Copper on Adsorption of Benzotriazole and Cl. Part I. *J. Phys. Chem. C* **2014**, *118*, 933−943.
(22) Roberts, R. F. X-ray photoelectron spectroscopic characterization of copper oxide surfaces treated with benzotriazole. *J. Electron Spectrosc. Relat. Phenom.* **1974**, *4*, 273−291.
(23) Rubim, J. C.; Gutz, I. G. R.; Sala, O.; Orvillethomas, W. Surface enhanced Raman-spectra of benzotriazole adsorbed on a copper electrode. *J. Mol. Struct.* **1983**, *100*, 571−583.
(24) Fang, B. S.; Olson, C. G.; Lynch, D. W. A photoemission-study of benzotriazole on clean copper and cuprous-oxide. *Surf. Sci.* **1986**, *176*, 476−490.
(25) Walsh, J. F.; Dhariwal, H. S.; Gutierrez-Sosa, A.; Finetti, P.; Muryn, C. A.; Brookes, N. B.; Oldman, R. J.; Thornton, G. Probing molecular orientation in corrosion inhibition via a NEXAFS study of benzotriazole and related molecules on Cu(100). *Surf. Sci.* **1998**, *415*, 423−432.
(26) Grillo, F.; Tee, D. W.; Francis, S. M.; Fruechtl, H.; Richardson, V. Initial stages of benzotriazole adsorption on the Cu(111) surface. *Nanoscale* **2013**, *5*, 5269−5273.
(27) Grillo, F.; Tee, D. W.; Francis, S. M.; Fruechtl, H. A.; Richardson, N. V. Passivation of Copper: Benzotriazole Films on Cu(111). *J. Phys. Chem. C* **2014**, *118*, 8667−8675.
(28) Velasco-Velez, J.-J.; Wu, C. H.; Pascal, T. A.; Wan, L. F.; Guo, J.; Prendergast, D.; Salmeron, M. The structure of interfacial water on gold electrodes studied by X-ray absorption spectroscopy. *Science* **2014**, *346*, 831−834.

DOI: 10.1021/acs.langmuir.8b03528
Langmuir 2019, 35, 882−893

(29) Ontaneda, J.; Nicklin, R. E. J.; Cornish, A.; Roldan, A.; Grau-Crespo, R.; Held, G. Adsorption of Methyl Acetoacetate at Ni111: Experiment and Theory. *J. Phys. Chem. C* **2016**, *120*, 27490−27499.
(30) Tsaousis, P.; Ontaneda, J.; Bignardi, L.; Bennett, R. A.; Grau-Crespo, R.; Held, G. Combined Experimental and Theoretical Study of Methyl Acetoacetate Adsorption on Ni100. *J. Phys. Chem. C* **2018**, *122*, 6186−6194.
(31) Fronzoni, G.; Balducci, G.; De Francesco, R.; Romeo, M.; Stener, M. Density Functional Theory Simulation of NEXAFS Spectra of Molecules Adsorbed on Surfaces: C_2H_4 on Si(100) Case Study. *J. Phys. Chem. C* **2012**, *116*, 18910−18919.
(32) Siefermann, K. R.; et al. Atomic-Scale Perspective of Ultrafast Charge Transfer at a Dye-Semiconductor Interface. *J. Phys. Chem. Lett.* **2014**, *5*, 2753−2759.
(33) Woodruff, D. P. Surface structure determination using X-ray standing waves. *Rep. Prog. Phys.* **2005**, *68*, 743.
(34) Fisher, C. J.; Ithin, R.; Jones, R. G.; Jackson, G. J.; Woodruff, D. P.; Cowie, B. C. C. Non-dipole photoemission effects in x-ray standing wavefield determination of surface structure. *J. Phys.: Condens. Matter* **1998**, *10*, L623−L629.
(35) Kresse, G.; Hafner, J. *Ab initio* molecular dynamics for liquid metals. *Phys. Rev. B* **1993**, *47*, 558−561.
(36) Kresse, G.; Hafner, J. *Ab initio* molecular-dynamics simulation of the liquid-metal-amorphous-semiconductor transition in germanium. *Phys. Rev. B* **1994**, *49*, 14251−14269.
(37) Kresse, G.; Furthmueller, J. Efficiency of ab-initio total energy calculations for metals and semiconductors using a plane-wave basis set. *Comput. Mater. Sci.* **1996**, *6*, 15−50.
(38) Kresse, G.; Furthmueller, J. Efficient iterative schemes for ab initio total-energy calculations using a plane-wave basis set. *Phys. Rev. B* **1996**, *54*, 11169−11186.
(39) Klimeš, J.; Bowler, D. R.; Michaelides, A. Van der Waals density functionals applied to solids. *Phys. Rev. B* **2011**, *83*, No. 195131.
(40) Kresse, G.; Joubert, D. From ultrasoft pseudopotentials to the projector augmented-wave method. *Phys. Rev. B* **1999**, *59*, 1758−1775.
(41) Köhler, L.; Kresse, G.; Schmid, M.; Lundgren, E.; Gustafson, J.; Mikkelsen, A.; Borg, M.; Yuhara, J.; Andersen, J. N.; Marsman, M.; Varga, P. High-coverage oxygen structures on Rh(111): Adsorbate repulsion and site preference is not enough. *Phys. Rev. Lett.* **2004**, *93*, No. 266103.
(42) Prendergast, D.; Galli, G. X-ray absorption spectra of water from first principles calculations. *Phys. Rev. Lett.* **2006**, *96*, No. 215502.
(43) Giannozzi, P.; et al. QUANTUM ESPRESSO: a modular and open-source software project for quantum simulations of materials. *J. Phys.: Condens. Matter* **2009**, *21*, No. 395502.
(44) Taillefumier, M.; Cabaret, D.; Flank, A.-M.; Mauri, F. X-ray absorption near-edge structure calculations with the pseudopotentials: Application to the K edge in diamond and α-quartz. *Phys. Rev. B* **2002**, *66*, No. 195107.
(45) Prendergast, D.; Louie, S. G. Bloch-state-based interpolation: An efficient generalization of the Shirley approach to interpolating electronic structure. *Phys. Rev. B* **2009**, *80*, No. 235126.
(46) Shirley, E. L. Optimal basis sets for detailed Brillouin-zone integrations. *Phys. Rev. B* **1996**, *54*, 16464−16469.
(47) Perdew, J. P.; Burke, K.; Ernzerhof, M. Generalized gradient approximation made simple. *Phys. Rev. Lett.* **1996**, *77*, 3865−3868.
(48) Vanderbilt, D. Soft Self-consistent pseudopotentials in a generalized eigenvalue formalism. *Phys. Rev. B* **1990**, *41*, 7892−7895.
(49) Stöhr, J. *NEXAFS Spectroscopy*; Springer Series in Surface Sciences; Springer-Verlag: Berlin, Heidelberg, 1992.
(50) Tanuma, S.; Powell, C. J.; Penn, D. R. Calculations of electron inelastic mean free paths. *Surf. Interface Anal.* **1991**, *17*, 911−926.
(51) Katritzky, A. R.; Wang, Z.; Tsikolia, M.; Hall, C. D.; Carman, M. Benzotriazole is thermally more stable than 1,2,3-triazole. *Tetrahedron Lett.* **2006**, *47*, 7653−7654.
(52) Walker, R. Benzotriazole as a corrosion inhibitor. *Met. Finish.* **1973**, *71*, 63−66.
(53) Koschel, H.; Held, G.; Steinruck, H. P. The growth of thin Cu layers on Ni(111) studied by CO titration and photoelectron spectroscopy. *Surf. Sci.* **2000**, *453*, 201−213.
(54) Nilsson, J.-O.; Törnkvist, C.; Liedberg, B. Photoelectron and infrared reflection absorption spectroscopy of benzotriazole adsorbed on copper and cuprous oxide surfaces. *Appl. Surf. Sci.* **1989**, *37*, 306−326.
(55) Kokalj, A.; Peljhan, S.; Koller, J. The Effect of Surface Geometry of Copper on Dehydrogenation of Benzotriazole. Part II. *J. Phys. Chem. C* **2014**, *118*, 944−954.
(56) Bougeard, D.; Le Calvé, N.; Saint Roch, B.; Novak, A. 1,2,4-Triazole: Vibrational spectra, normal coordinate calculations, and hydrogen bonding. *J. Chem. Phys.* **1976**, *64*, 5152−5164.
(57) Liu, D.-J.; Walen, H.; Oh, J.; Lim, H.; Evans, J. W.; Kim, Y.; Thiel, P. A. Search for the structure of a sulfur-induced reconstruction on Cu(111). *J. Phys. Chem. C* **2014**, *118*, 29218−29223.
(58) Muñoz-Márquez, M. A.; Parkinson, G. S.; Quinn, P. D.; Gladys, M. J.; Tanner, R. E.; Woodruff, D. P.; Noakes, T. C. Q.; Bailey, P. N-induced pseudo-(100) reconstruction of Cu(111): One layer or more? *Surf. Sci.* **2005**, *582*, 97−109.
(59) Moritani, K.; Okada, M.; Teraoka, Y.; Yoshigoe, A.; Kasai, T. Reconstruction of Cu(111) induced by a hyperthermal oxygen molecular beam. *J. Phys. Chem. C* **2008**, *112*, 8662−8667.
(60) Grönbeck, H. Thiolate induced reconstruction of Au(111) and Cu(111) investigated by density functional theory calculations. *J. Phys. Chem. C* **2010**, *114*, 15973−15978.

DOI: 10.1021/acs.langmuir.8b03528
Langmuir 2019, 35, 882−893